IX CONGRESSO BRASILEIRO DE
ENGENHARIA E CIÊNCIAS TÉRMICAS

9th BRAZILIAN CONGRESS OF THERMAL
ENGINEERING AND SCIENCES

Paper CIT02-0622

# RECTANGULAR OBSTRUCTION THERMAL EFFECTS ON ENTRANCE REGIONS OF FLAT PLATE CHANNELS

**Aldélio Bueno Caldeira**
Universidade Federal do Rio de Janeiro, Programa de Engenharia Mecânica - 21945-970 – Rio de Janeiro - RJ - Brazil
aldelio@lmt.coppe.ufrj.br

**Albino José Kalab Leiroz**
Instituto Militar de Engenharia, Departamento de Engenharia Mecânica e de Materiais - 22290-270 – Rio de Janeiro – RJ - Brazil
leiroz@ime.eb.br

**Helcio Rangel Barreto Orlande**
Universidade Federal do Rio de Janeiro, Programa de Engenharia Mecânica - 21945-970 – Rio de Janeiro - RJ - Brazil
helcio@serv.ufrj.br

***Abstract.*** *Conjugate thermal effects of rectangular obstructions on entrance regions of parallel plate channels are numerically investigated in the present work. The incompressible laminar flow governing equations, written in vorticity-stream function formulation, as well as the energy conservation equation are discretized with a hybrid finite difference scheme. The domain is subdivided into zones and a regular mesh is used within the obtained subdomains. Constant temperature and constant heat flux boundary conditions are considered in the present study for the channel walls. Results are obtained for fully developed and uniform inlet velocity profiles. The effects of the obstruction thickness, height, and thermal diffusivity on the temperature field and Nusselt number are analyzed. The numerical results obtained here are validated with limiting analytical solutions available in the literature.*

***Keywords.*** *conjugate heat transfer, rectangular obstruction, entrance region, parallel flat plate.*

## 1. Introduction

The study of internal convection effects within parallel plate channels share the interest of basic and applied research. The design and development of flame holders for combustion devices (Williams, 1985, and Esquiva-Dano et al., 2001), the cooling of electronic systems (Davallah and Bayazitoglu, 1987), fouling and fins in heat exchangers (Kern, 1965) and thermal intrusive aspects of measurement devices (Holman, 1989) are among the applications motivating the study of the rectangular obstructions inside parallel plate channel.

The analysis of flows in parallel plate channels with periodic rod obstructions and constant wall temperature was presented by Yuan et al. (1998). In this numerical work, the solution of the *momentum* and energy conservation equations were obtained with periodic boundary conditions and the results indicate an abrupt decrease in the Nusselt number in the near field upstream of rods, followed by an abrupt increase in the region downstream of rod. Periodic internal ribs inside tubes were also studied (Weeb et al., 1971), leading to friction factor and heat transfer coefficient correlations, based on the law of the wall and on the heat-*momentum* transfer analogy. Rowley and Patankar (1984) presented a numerical work on periodic circular internal fins inside tubes. The friction and heat transfer process were analyzed, using the Nusselt and Prandtl numbers and emphasizing the ratio of the length between two periodic fins by the height of the fin. The results indicated that the presence of fins inside tubes do not always lead to heat transfer enhancement, due to the induced flow distortion caused by the extended surfaces. Therefore, the flow distortion can substantially reduce the heat transfer from the wall.

The conjugate thermal problem, considering an annular turbulent flow inside a concentric circular arrangement with periodic internal fins, was investigated by Andrade and Zaparoli (1999). Reverse heat transfer between fluid and solid boundary was observed near fin-tube corner. The results show that the reverse heat flux was enhanced for increasing the Reynolds number. However, an increase of the solid/ fluid conductivity ratio leads to a decrease of the reverse heat flux. The reverse heat flux is attributed to the low value of the temperature at the fin–tube corner and to the recirculating fluid.

A conjugate heat transfer problem within an array of rectangular obstructions inside a parallel plate channel was studied by Davalath et al. (1987) by using a finite difference approach. In order to model electronic components on a horizontal circuit board, the array of heat generating obstructions was placed on one of the channel walls. Effects of the Reynolds number and the space between obstructions on the heat transfer process and fluid flow were examined.

The effects of rectangular obstructions inside parallel plate channels on entrance regions was numerically studied by Caldeira et al. (2001). The objective was modeling the intrusive aspects of orifice plate devices into thermal and

fluid flow. The influence of Reynolds number, obstruction thickness, height and asymmetry, considering constant wall temperature or heat flux boundary conditions were evaluated. The results showed that there was a strong relationship between the recirculation zones and the heat transfer phenomena, based on the Nusselt number behavior along the channel and obstruction walls. Conjugate heat transfer was not considered in that work.

In the present work, conjugate heat transfer effects of a symmetric rectangular obstruction on the hydrodynamical and thermal entrance regions within parallel plate channels are studied. The rectangular obstruction thermal effects are analyzed using the temperature field and the Nusselt number evaluated along the channel and obstruction walls. Heat transfer enhancement due to the obstruction, which presents an internal fin effect, and the conduction heat transfer within the obstruction are also analyzed. The laminar incompressible flow governing equations written in vorticity-stream function form are discretized with an implicit first order accurate finite difference scheme (Anderson et al., 1984). The physical solution domain is divided into zones and regular discretizing grids are used within the obtained subdomains. The resulting system of algebraic equations is solved by an iterative procedure with local error control (Anderson et al., 1984). Constant wall temperature and constant wall heat flux boundary conditions are considered for the channel walls. The Graetz problems (Kays and Crawford, 1980 and Cotta and Ozisik, 1986) are used to validate the obtained numerical results.

## 2. Mathematical Formulation

It is note worthy that the proposed physical-mathematical model only considers the heat transfer into the fluid and solid obstruction. So, the conduction through the channel walls is not taken into account in the present work.

The solution domain is depicted in Fig. (1), with the principal geometric dimensions, which also shows the Cartesian system of coordinates used in the present work.

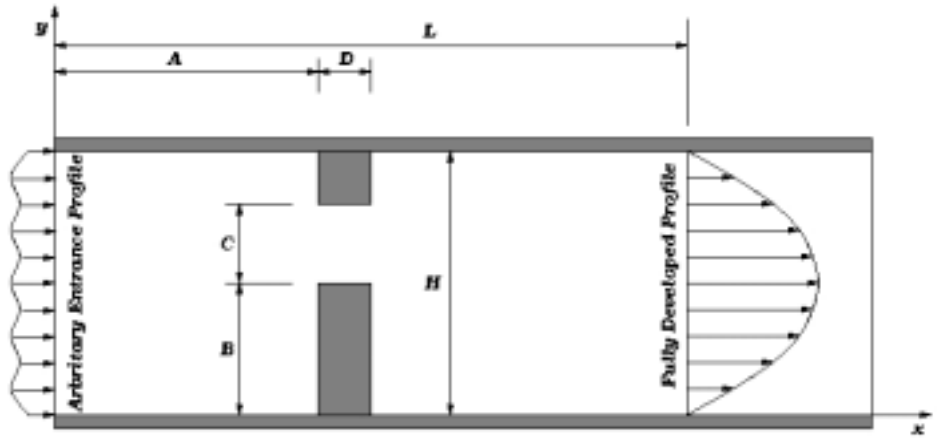


Figure 1 – Physical domain and principal dimensions.

The dimensionless system of equations for the conservation of mass and *momentum*, for the fluid domain, considering laminar and incompressible flow inside the channel, and the energy, for the fluid and solid domains, are written as

$$\frac{\partial u_x}{\partial x}+\frac{\partial u_y}{\partial y}=0 \tag{1}$$

$$\frac{\partial u_x}{\partial t}+\frac{\partial u_x u_x}{\partial x}+\frac{\partial u_y u_x}{\partial y}=-\frac{\partial P}{\partial x}+\frac{1}{Re}\left(\frac{\partial^2 u_x}{\partial x^2}+\frac{\partial^2 u_x}{\partial y^2}\right) \tag{2}$$

$$\frac{\partial u_y}{\partial t}+\frac{\partial u_y u_x}{\partial x}+\frac{\partial u_y u_y}{\partial y}=-\frac{\partial P}{\partial y}+\frac{1}{Re}\left(\frac{\partial^2 u_y}{\partial x^2}+\frac{\partial^2 u_y}{\partial y^2}\right) \tag{3}$$

$$\frac{\partial \theta}{\partial t}+\frac{\partial u_x \theta}{\partial x}+\frac{\partial u_y \theta}{\partial y}=\frac{\partial}{\partial x}\left(\frac{1}{Pe^*}\frac{\partial \theta}{\partial x}\right)+\frac{\partial}{\partial y}\left(\frac{1}{Pe^*}\frac{\partial \theta}{\partial y}\right) \tag{4}$$

with boundary conditions

$$u_x = f_i(y), \quad u_y = 0, \quad \theta = 1; \quad x = 0, \ 0 \le y \le 1 \tag{5}$$

$$u_x = f_o(y), \quad u_y = 0, \quad \partial\theta/\partial x = \partial\theta_w/\partial x; \quad x \to \infty, \; 0 \le y \le 1 \tag{6}$$

$$u_x = 0 \;\; , \; u_y = 0 \;\; ; \quad 0 \le x \le \infty \; ; \quad at \quad h_l(x,y) \quad and \quad h_u(x,y) \tag{7}$$

$$a_l\,\theta + b_l\,\partial\theta/\partial y = \varphi_l\,; \quad 0 \le x \le \infty \;\; , \;\; y = 0 \tag{8}$$

$$a_u\,\theta - b_u\,\partial\theta/\partial y = \varphi_u\,; \quad 0 \le x \le \infty \;\; , \;\; y = 1 \tag{9}$$

The constants $a_l$, $b_l$, $a_u$, $b_u$, $\varphi_l$ and $\varphi_u$ appearing in Eq.(8-9) will be set accordingly with the kind of boundary condition being considered for each case.

The initial conditions are given by

$$u_x = 0 \;\; , \; u_y = 0 \;\; , \; \theta = 0 \;\; ; \quad 0 \le x < \infty \;\; , \; 0 < y < 1 \tag{10}$$

The functions $h_l(x,y)$ and $h_u(x,y)$, appearing in Eq.(7), describe the lower and upper irregular solid surfaces are defined as

$$h_l(x,y) = \begin{cases} y = 0; \quad 0 \le x < A/H \\ x = A/H; \quad 0 \le y \le B/H \\ y = B/H; \quad A/H < x < (A+D)/H \\ x = (A+D)/H; \quad 0 \le y \le B/H \\ y = 0; \quad (A+D)/H < x < \infty \end{cases} \tag{11}$$

and

$$h_u(x,y) = \begin{cases} y = 1; \quad 0 \le x < A/H \\ x = A/H; \quad (B+C)/H \le y \le 1 \\ y = (B+C)/H; \quad A/H < x < (A+D)/H \\ x = (A+D)/H; \quad (B+C)/H \le y \le 1 \\ y = 1; \quad (A+D)/H < x < \infty \end{cases} \tag{12}$$

The dimensionless variables appearing in Eqs. (1-10) are defined as

$$x = \frac{X}{H}\,; \; y = \frac{Y}{H}\,; \; u_x = \frac{U_X}{U_{max}}\,; \; u_y = \frac{U_Y}{U_{max}}\,; \; p = \frac{P}{\rho(U_{max})^2}\,; \; \theta = \frac{T_c - T}{T_c - T_i}\,; \; t = \frac{t^*}{H/U_{max}} \tag{13}$$

where the channel height $(H)$ and the maximum velocity at the outlet $(U_{max})$ are used as length and velocity characteristic quantities, respectively. The dimensionless temperature $(\theta)$ is defined in terms of a constant characteristic temperature, $T_c$, and of a constant inlet temperature, $T_i$. For the constant wall temperature case, $T_c$, is defined as the wall temperature value, $T_w$. For constant wall heat flux boundary condition, the characteristic temperature is defined as $q_w^*/(k\,H)$.

The Reynolds (*Re*) and Peclet ($Pe^*$) numbers are defined as

$$Re = \frac{U_{max}\,H}{\nu}\,; \tag{14}$$

$$Pe^* = \begin{cases} Pe = \dfrac{U_{max}\,H}{\alpha} \\ Pe_s = \dfrac{U_{max}\,H}{\alpha_s} \end{cases} \tag{15}$$

where $\nu$, $\alpha$ and $\alpha_s$ represent the kinematic viscosity, the fluid and solid thermal diffusivities, respectively. *Pe* is the fluid Peclet number and $Pe_s$ is an artificial Peclet number for the solid obstruction. Note that $Pe_s$ is just introduced in order to maintain the same dimensionless space and time scales on the solid and fluid subdomains.

The flow governing equations are rewritten in dimensionless vorticity-stream function form as

$$\frac{\partial \xi}{\partial t} + \frac{\partial u_x\, \xi}{\partial x} + \frac{\partial u_y\, \xi}{\partial y} = \frac{1}{Re}\left( \frac{\partial^2 \xi}{\partial x^2} + \frac{\partial^2 \xi}{\partial y^2} \right) \tag{16}$$

$$-\xi = \frac{\partial^2 \psi}{\partial x^2} + \frac{\partial^2 \psi}{\partial y^2} \tag{17}$$

with boundary conditions

$$\psi = \int_0^y f_i(y)\,dy; \quad x = 0,\ 0 \le y \le 1 \tag{18}$$

$$\psi = \int_0^y f_o(y)\,dy; \quad x \to \infty,\ 0 \le y \le 1 \tag{19}$$

$$\psi = 0; \quad 0 \le x \le \infty \ , \quad at \quad h_l(x,y) \tag{20}$$

$$\psi = \int_0^1 f_i(y)\,dy; \quad 0 \le x \le \infty \ , \quad at \quad h_u(x,y) \tag{21}$$

and initial conditions

$$\psi = 0\ ,\ \xi = 0\ ;\ 0 \le x < \infty\ ,\ h_l(x,y) < y < h_u(x,y) \tag{22}$$

Vorticity ($\xi$) and stream function ($\psi$) are respectively defined in terms of the longitudinal and transversal velocity components as

$$\xi = \frac{\partial u_y}{\partial x} - \frac{\partial u_x}{\partial y} \tag{23}$$

and

$$u_x = \frac{\partial \psi}{\partial y}, \quad u_y = -\frac{\partial \psi}{\partial x} \tag{24}$$

The vorticity values along the solid boundaries and at the channel inlet and outlet are initially unknown. These quantities are determined by an iterative solution procedure of the flow equations, which also accounts for the treatment of the non-linear terms appearing in Eq. (16) (Anderson et al., 1984).

## 3. Numerical Aspects

In the present work, the finite differences method was used for the numerical solution of the governing equations previously described. The semi-infinite physical domain was truncated at $x = L / H$ where the outlet boundary conditions were applied. Numerical tests were performed for different values of $L$ in order to guarantee independence of the truncated domain length. The truncated domain length was considered satisfactory when the deviation between the numerical Nusselt number in the end of the channel and the analytical Nusselt number (Kays and Crawford, 1980) for thermal developed flow were smaller than *1%*. A hybrid scheme (Versteeg and Malalasekera, 1995) was employed to discretize the transport equations. Furthermore, despite the transient nature of equations being solved, only the steady state results were analyzed in the present work.

The solution domain was split into five subdomains as shown in Fig. (2). Regularly spaced points were used within the subdomains, defining the discretizing grid. The resulting system of algebraic equations was solved by an iterative Gauss-Seidel procedure with sub-relaxation (Anderson et al., 1984). In order to address the unknown vorticity values along the solution domain boundaries, an iterative procedure was employed. Initially, estimated vorticity values along the boundary were defined, allowing the solution of the vorticity transport equation, Eq. (16). With the obtained results, Eq. (17) was solved leading to the stream function distribution within the domain. Applying the velocity boundary conditions, stream function, vorticity and the definitions in terms of the primitive variables, a vorticity distribution along the solid boundaries was calculated. The obtained results allow the validation or correction of the initially estimated vorticity values. The iterative procedure was repeated until a specified tolerance criterion was satisfied. The solution was then marched in time.

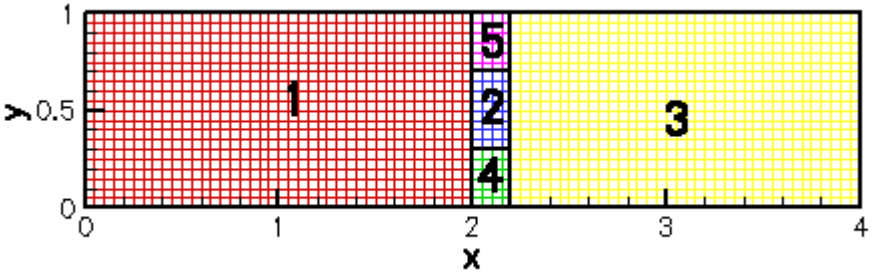


Figure 2 – Discretizing grid showing the five subdomains.

The numerical solution proceeds until the obtained vorticity and temperature fields for two consecutive time steps differ by an amount smaller than a given steady state tolerance.

The Nusselt number along the channel walls is defined in terms of the dimensionless quantities by

$$Nu = \frac{2}{\theta_b - \theta_w} \left. \frac{\partial \theta}{\partial y} \right|_{y = h_l} \tag{25}$$

where the dimensionless bulk temperature $\theta_b$ is defined by

$$\theta_b = \frac{\int_{h_l}^{h_u} (\theta\, u_x)\, dy}{\int_{h_l}^{h_u} u_x\, dy} \tag{26}$$

## 4. Results

The analytical solutions of Kays and Crawford (1980), considering constant temperature in the channel walls, and of Cotta and Ozisik (1986), considering constant heat flux in the channel walls, for the Graetz problems were used to validate the proposed numerical procedure. Graetz problems consider a fully developed velocity and a developing temperature profiles inside parallel plate channels without obstructions. The formulation described by the Eqs. (1-10) leads to the Graetz problem formulation as the rectangular obstruction height, or thickness, vanishes. Inlet and outlet velocity profiles were defined as $f_i(y) = 4y - 4y^2$ and $f_o(y) = 4y - 4y^2$, respectively. Constant wall temperature, or first kind, ($a_u = a_l = 1, b_u = b_l = 0, \varphi_l = \varphi_u = \theta_w = 0$) and constant wall heat flux, or second kind, ($a_u = a_l = 0, b_u = b_l = 1, \varphi_l = \varphi_u = q_w = \textit{arbitrary constant value}$) thermal boundary conditions were considered. For the present analysis, the inlet and outlet temperature profiles were considered as uniform and fully developed, respectively.

Table (1) shows the comparison between the present numerical results for the Nusselt number along the channel wall for the Graetz problems with the analytical results of Kays and Crawford (1980) and Cotta and Ozisik (1986), considering the cases of the first and second kind boundary conditions. Deviations smaller than *1,5%* between the numerical and analytical results are observed in Tab. (1).

The numerical results presented in Tab (1) were obtained by using a grid with *401* and *41* points along the *x* and *y* directions, respectively.

Table 1 - Nusselt number in the thermal developing region of the Graetz problems.

| | *Nu* ($\theta_w$ = *constant*) | | *Nu* ($q_w$ = *constant*) | |
|---|---|---|---|---|
| *x* | *Numerical* | *Kays and Crawford, 1980* | *Numerical* | *Cotta and Ozisik, 1986* |
| *4/3* | *8.61* | *8.52* | *10.1186* | *9.9878* |
| *8/3* | *7.77* | *7.75* | *8.8667* | *8.8031* |
| *20/3* | *7.55* | *7.55* | *8.2908* | *8.2783*[*] |
| $\infty$ | *7.54* | *7.54* | *8.2556* | *8.2353* |

[*] interpolated value.

Results obtained for symmetrical rectangular obstruction are shown below. The geometric and physical parameters for a base case are shown in Tab (2). The base case considers the developed velocity profile at the channel inlet and the constant channel wall temperature.

Table 2 - Geometric and physical parameters for a base case.

| *Geometric Parameters* | | | | *Physical Parameters* | | |
|---|---|---|---|---|---|---|
| *A/H* | *B/H* | *C/H* | *D/H* | *Re* | *Pe* | $Pe_s$ |
| *2* | *0.35* | *0.3* | *0.3* | *100* | *100* | *100* |

Figures (3-4) show the effect of the inlet velocity profile on the flow field results. The fully developed inlet velocity profile ( $f_i(y) = 4y - 4y^2$ ) on Fig. (3) leads to parallel streamlines in the channel inlet. For uniform velocity inlet profile ( $f_i(y) = 2/3$ ), Fig. (4) shows developing boundary layers along the channel inlet.

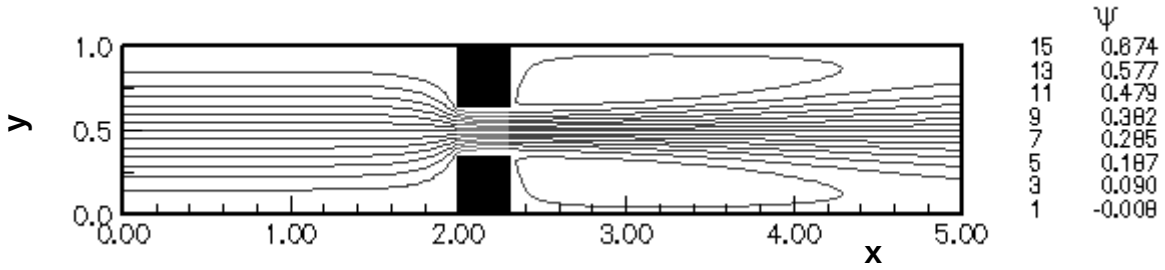


Figure 3 – Stream function considering the developed inlet velocity profile (*C/H = 0.3, D/H = 0.3, Re = 100*).

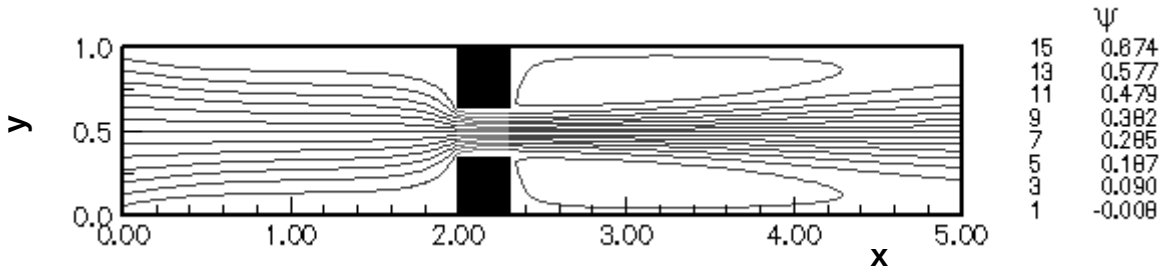


Figure 4 – Stream function considering uniform inlet velocity profile (*C/H = 0.3, D/H = 0.3, Re = 100*).

The temperature fields are presented in Figs. (5-10) for different values of geometric parameters (throat width, *C/H*, and thickness, *D/H*) and physical parameters (*Re*, *Pe* and $Pe_s$).

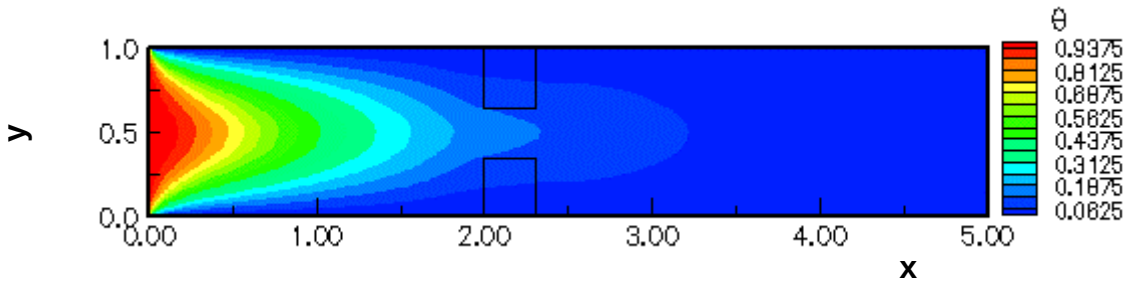


Figure 5 – Temperature field considering the developed inlet velocity profile – constant wall temperature (*C/H = 0.3, D/H = 0.3, Pe = 10* and $Pe_s = 10$).

Comparing Fig. (5) and Fig. (6), which corresponds to the base case, it is possible to analyze the influence of the *Pe* on the temperature field when the ratio $Pe/Pe_s$ is maintained constant and equal to *1*. In Fig. (5) – *Pe = 10* - diffusion dominates the heat transfer process. Then, the fluid and the solid reach small values of $\theta$ into a short length of the channel. In Fig. (6) – *Pe = 100* - the convection effects become important and high values of $\theta$ can be observed in the fluid domain downstream of the rectangular obstruction and in the solid domain.

The effect of the solid diffusivity on the obstruction is shown in Figs. (6-8), considering *Pe = 100.* Then, for a constant value of *Pe*, the solid diffusivity reduces when the $Pe_s$ increases. Fig. (7) shows the case where the diffusivity is sufficiently high - $Pe_s = 1$ – to guarantee that temperature in the obstruction is basically uniform and equal to the wall temperature. In Fig. (6) - $Pe_s = 100$ - the effect of the channel wall temperature is not so intense when compared to results shown in Fig. (7) and the temperature of the fluid increases the value of $\theta$ in solid regions. Fig. (8) shows the case where the diffusivity is low enough - $Pe_s = 10000$ - to make the solid approximately adiabatic which is indicated by the almost vanishing heat flux at the obstruction/ fluid interface. This effect can be specially observed

behind the obstruction in the longitudinal direction when Figs. (6-8) are compared. The thermal effect of the obstruction on the temperature field increases with the solid diffusivity. Furthermore, diffusion dominates the heat transfer into the regions behind the obstruction, which is linked with the hydrodynamical effect of the recirculation zone. These effects can also be observed in the region upstream of the obstruction, the stagnant fluid regions. Fig. (7) coincides with the case with constant wall boundary condition established along of all solid/ fluid interface present in Caldeira et al. (2001).

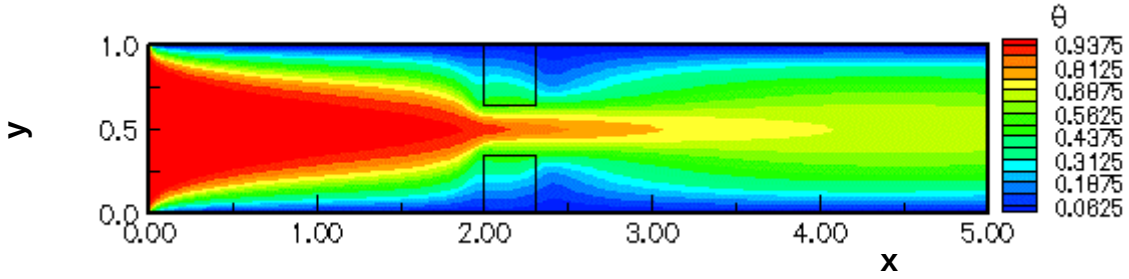


Figure 6 – Temperature field considering the developed inlet velocity profile - constant wall temperature (*C/H = 0.3, D/H = 0.3, Pe = 100* and $Pe_s = 100$) – *Base Case*.

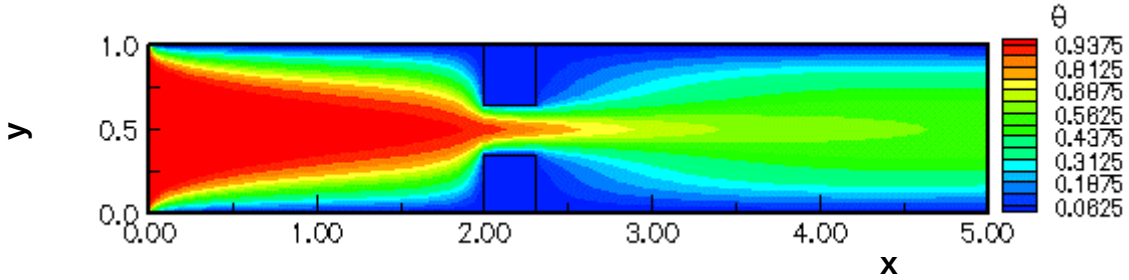


Figure 7 – Temperature field considering the developed inlet velocity profile – constant wall temperature (*C/H = 0.3, D/H = 0.3, Pe = 100* and $Pe_s = 1$).

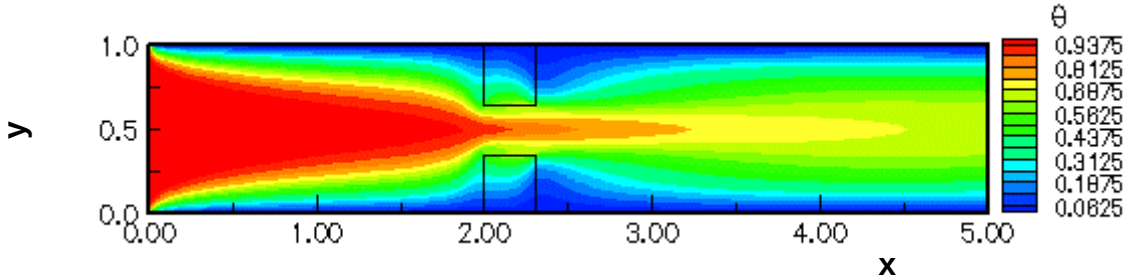


Figure 8 – Temperature field considering the developed inlet velocity profile – constant wall temperature (*C/H = 0.3, D/H = 0.3, Pe = 100* and $Pe_s = 10000$).

The effect of the obstruction geometry is analyzed in Figs. (6, 9-10). These figures show that the disturbance on the temperature field increases as obstruction dimensions are enlarged. The regions with low values of temperature increase into the fluid domains with the dimension of the obstruction, because of the improvement of the diffusion in recirculation zones and of the greater heat transfer areas at obstruction/ fluid interface.

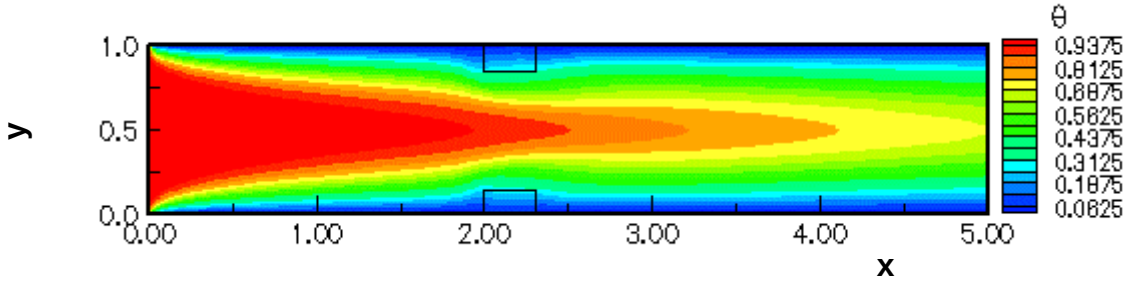


Figure 9 – Temperature field considering the developed inlet velocity profile – constant wall temperature (*C/H = 0.7, D/H = 0.3, Pe = 100* and $Pe_s = 100$).

Figure (11) presents the effects of the physical parameter $Pe_s$ on the Nusselt number when the *Pe* is equal to *100*, considering the base case, boundary conditions and geometric parameters (see Tab. (2)). In Fig. (11a) the Nusselt number is practically independent of the $Pe_s$ downstream and upstream of the obstruction. However, at the end of the

first subdomain and at the beginning of the third subdomain (see Fig. (2)) the Nusselt number presents a lower value for $Pe_s = 1$ and a greater value for $Pe_s = 100$. In these regions, the diffusive heat transfer process is dominant because of the low fluid velocity values in the stagnant and recirculation zones (Caldeira et al., 2001). Then, for $Pe_s = 1$ the higher thermal diffusivity in the obstruction resulted on a temperature almost equal to zero along of the solid surfaces, inducing the reduction of the temperature in the longitudinal direction of the channel, attenuating the transversal temperature gradients downstream and upstream of the obstruction and, consequently, reducing the Nusselt number. A similar heat transfer phenomenon is observed for $Pe_s = 100$, but with less intensity than for $Pe_s = 1$, because the diffusivity decreases when $Pe_s$ increases. For $Pe_s = 10000$ the diffusivity of the obstruction is so low that the heat flux is drastically reduced at the obstruction/ fluid interface.

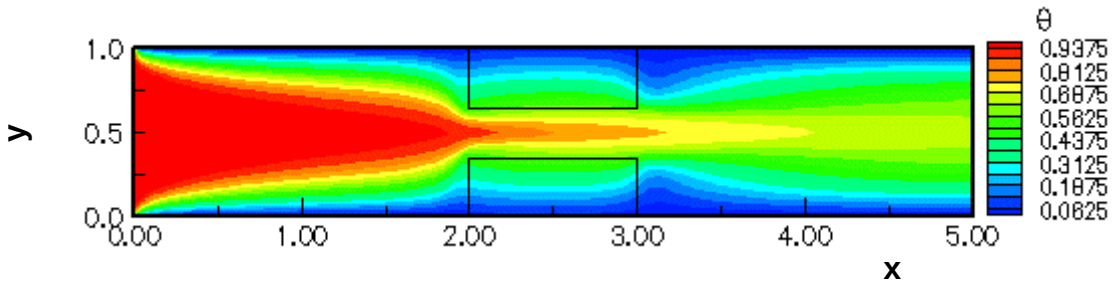


Figure 10 – Temperature field considering the developed inlet velocity profile – constant wall temperature (*C/H = 0.3, D/H = 1.0, Pe = 100* and $Pe_s = 100$).

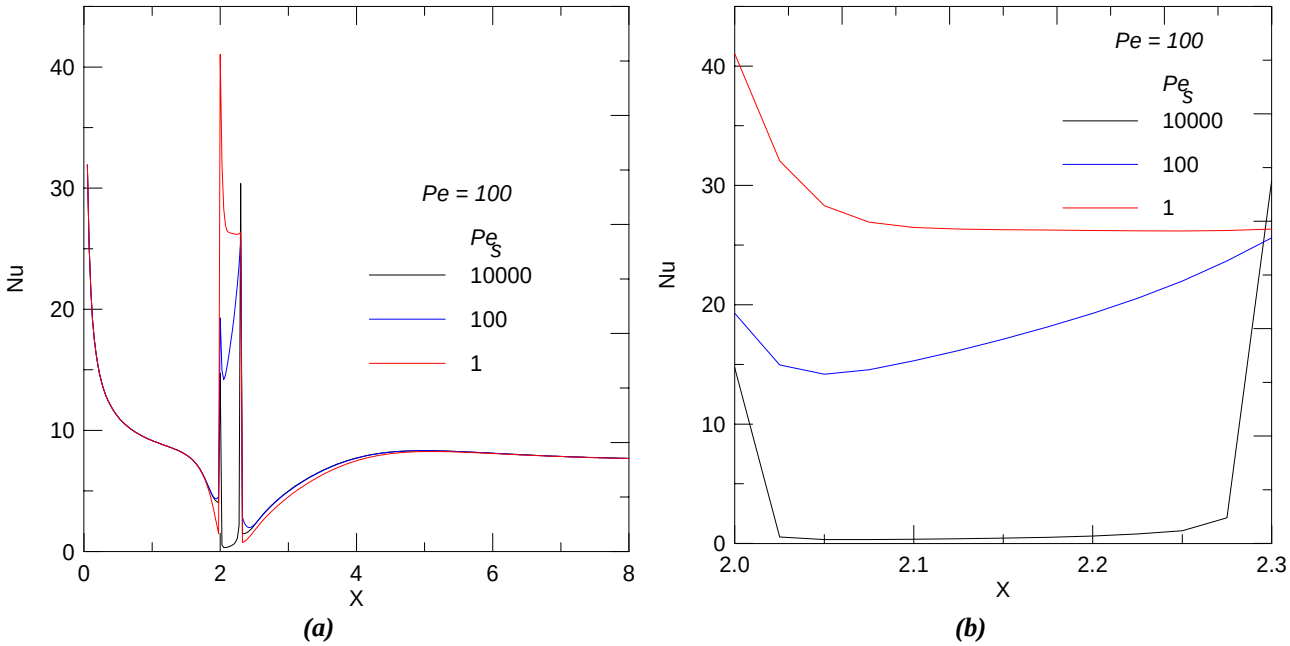


Figure 11 – ***(a)*** Effects of $Pe_s$ on Nusselt number along the channel. ***(b)*** Effects of $Pe_s$ on Nusselt number along the obstruction.

Figure (11b) shows the Nusselt number behavior on the second subdomain (see Fig. (2)) considering the same parameters and boundary conditions employed in Fig. (11a). In Fig. (11b) the convective heat transfer process is dominant, because of the high fluid velocity values in the throat. Furthermore, different behaviors are observed for each Nusselt curve. Analyzing Figs. (11b, 6, 7 and 8) it is possible to observe that the Nu behavior for each $Pe_s$ has an inverse correspondence with the temperature field in the obstruction. In other words, the temperature gradient in the fluid increases when the temperature in the obstruction decreases.

Figure (12a) shows the influences of geometric parameters on the Nusselt number along the channel, considering the base case, boundary conditions and physical parameters (Tab. (2)). Similarly to the cases presented in Fig. (11a) the Nu curves are practically not influenced by the geometric parameters in the first and third subdomains (Fig. (2)). In the second subdomain (Fig. (2)) the behavior of the Nusselt curves are similar to that described in the analysis of the Fig. (11b). The wide obstruction induces higher Nu in the outlet throat, because the transversal temperature gradient increases along the throat. But, the increasing ratio of the Nu curve is greater for the base case. Because in this case the distance between stagnant and recirculation zones are smaller than for *D/H = 1* case. Then, the longitudinal temperature gradient is greater for the base case. For *C/H = 0.7*, the large throat reduces the velocity gradient and the convection effect on the obstruction, reducing the Nu value.

Figure (12b) shows the effect of the boundary conditions on the Nusselt number for the physical and geometric parameters of the base case. The curves in Fig. (12b) presents an expected behavior. A larger Nu is observed for constant channel wall heat flux and into the first subdomain (Fig. (2)) the Nu for the uniform inlet velocity is a little greater than for the developed inlet boundary condition, because of the higher velocity gradients at channel walls inducing higher convection effects. The behavior of the curve of Fig. (12b) in the second subdomain (Fig. (2)) is similar to the Fig. (11b).

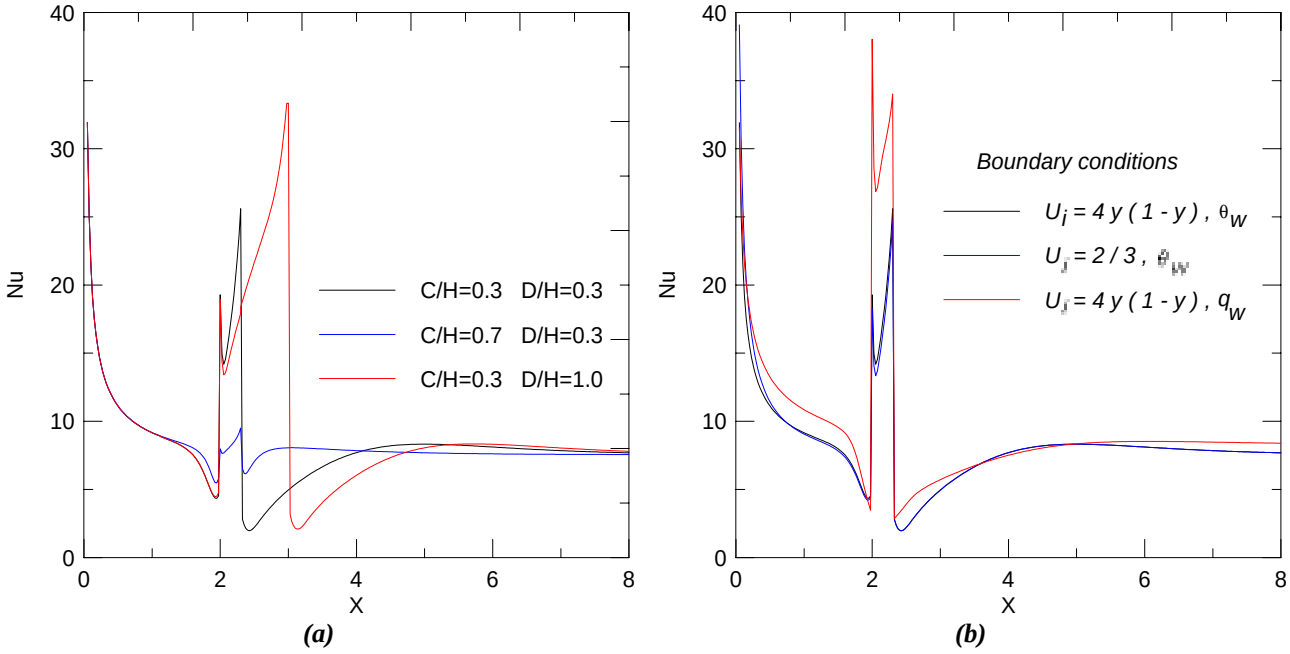


Figure 12– ***(a)*** Effects of the obstruction dimensions on Nusselt number. *(b)* Effects of boundary conditions on Nusselt number.

A unexpected behavior is presented in Fig. (13) where the *Pe* effects on the Nusselt number and on the temperature field behavior are evaluated, considering $Pe/Pe_s = 1$ and the base case (Tab. (2)) geometric parameters and boundary conditions.

In the Fig. (13a) the Nusselt number increases, in the second subdomain (Fig. (2)) when *Pe* decreases. This effect can be explained by the difference between the bulk temperature and the wall temperature on the obstruction associated with the heat flux behavior at obstruction/ fluid interface presented in Fig. (13b). From Eq. (25) the Nusselt number decreases when the difference between the bulk temperature and the wall temperature increases or when the heat flux at solid/ fluid interface decreases. In Fig. (13b) is possible to observe that both the difference between the bulk temperature and the wall temperature and the temperature gradient at solid/ fluid interface have low values for $Pe = 10$. On the other hand, it is also possible to observe that the ratio of the heat flux at solid/ fluid interface by the difference between the bulk temperature and the wall temperature is greater for $Pe = 10$. Therefore, the behavior of the Nusselt number, in the second subdomain is physically explained by the approximately uniform temperature field in such subdomain presented in Fig. (5) – $Pe = 10$ - which increases Nu.

Figure (13a) shows that in the first subdomain the Nusselt curve reaches the asymptotic behavior of the thermal developed condition for $Pe = 10$, being disturbed in the vicinities of the obstruction. However, for $Pe = 100$ the thermal developed condition is not reached, in the first subdomain. Although, both curves reaches the thermal developed condition in the third subdomain, as well as for all of the cases studied in this work. Comparing the curves in Fig. (13b) in the third subdomain, an overshooting is observed for $Pe = 100$, which is associated with the more intense recirculation zone for $Pe = 100$ than for $Pe = 10$ (Caldeira et al., 2001).

## 5. Conclusions

The present study shows the influence of rectangular obstructions on the thermal and hydrodynamical entrance regions inside parallel plate channels, by taking into account the conjugate heat transfer problem with the obstructions. The obtained results were used to evaluate quantitative and qualitatively the effects of the boundary conditions, as well as of geometric (*C/H* and *D/H*) and physical (*Re*, *Pe* and $Pe_s$) parameters of the rectangular symmetric obstruction on the flow and temperature fields. Results show that variations of these geometric and flow conditions have strong influence on the *momentum* and energy transfer mechanisms. The introduction of the conjugate effect of the obstruction shows the influence of the solid diffusivity on the temperature field and on Nusselt number behavior. Results show that by increasing the *Pe* number, the Nusselt number could be reduced. By reducing the $Pe_s$ number, the Nusselt number increases on the obstruction. Furthermore, by considering the constant wall boundary condition, when $Pe/Pe_s = 100$,

the temperature field is analogous to the temperature field obtained for the problem considering the constant solid/ fluid temperature boundary condition. On the other hand, for *Pe/ Pe$_s$ = 0.01* the heat flux at obstruction/ fluid interface almost vanishes.

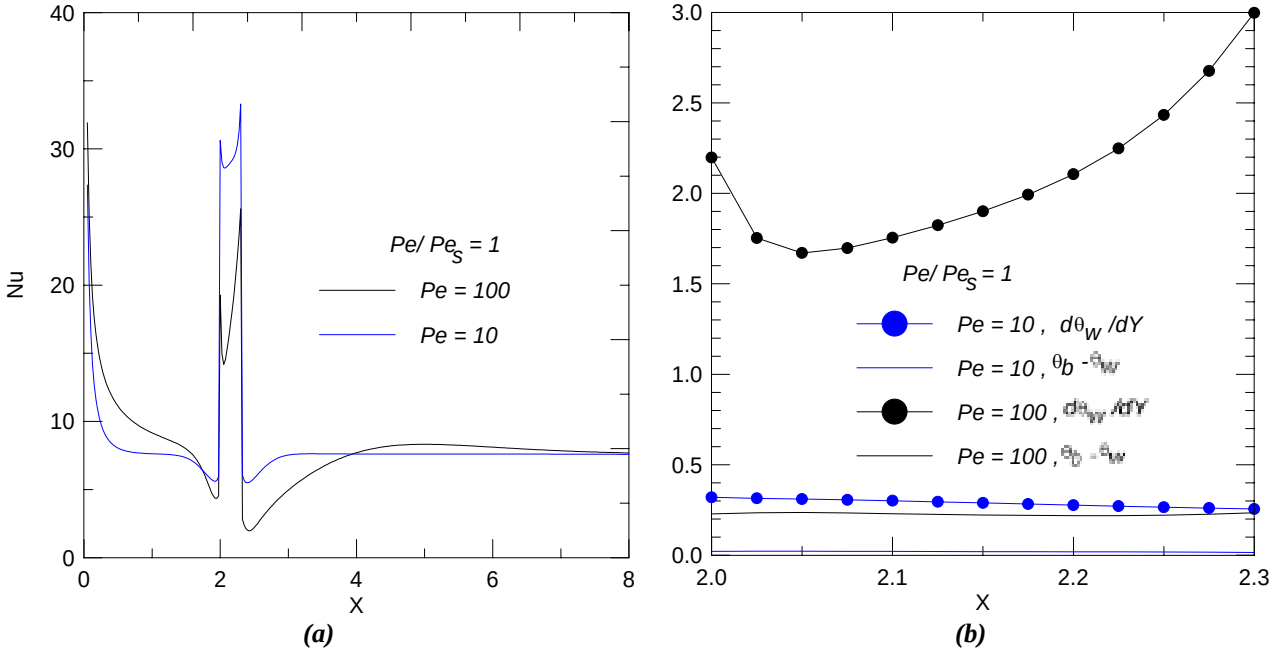


Figure 13 – ***(a)*** Effects of the *Pe* on Nusselt number for *Pe/ Pe$_s$ = 1*. *(b)* Behavior of the dimensionless heat flux, on the fluid/ obstruction interface, and of the $\theta_b$ - $\theta_w$.

## 6. References


Anderson, D.A., Tannehill, J.C. and Pletcher, R.H., 1984, "Computational Fluid Mechanics and Heat Transfer", Ed. Hemisphere Publishimg Corporation, New York, USA.

Andrade, C.R. and Zaparoli, E.L., 1999, "Occurrence of Reverse Heat Flux in Conjugated Heat Transfer in Finned Concentric Tubes", Proceedings of the 15th Brazilian Congress of Mechanical Engineering, CD-ROM, Rio de Janeiro, Brazil.

Caldeira, A. B., Rodrigues, R.C. and Leiroz, A., J. K., 2001, "Orifice Plate Effects On Hydrodynamical and Thermal Entrance Regions Inside Flat Channels", Proceedings of the 16th Brazilian Congress of Mechanical Engineering, CD-ROM, Uberlândia, Brazil, pp. 285-292.

Cotta, R. M., Ozisik, M. N., 1986, "Laminar Forced Convection to Non-Newtonian Fluids in Ducts with Prescribed Wall Heat Flux", International Communication in Heat and Mass Transfer, Vol. 13, n 3, pp. 325-334.

Davallah, J. and Bayazitoglu, Y, 1987, "Forced Convection Cooling Across Rectangular Blocks", J. Heat Trans. ASME, Vol. 109, pp. 321-328.

Esquiva-Dano, I., Nguyen, H. T. and Escudie, D., 2001, "Influence of Bluff-body's Shape on the Stabilization Regime of Non-premixed Flames", Combustion and Flame, Vol. 127, n 4, pp. 2167-2180.

Holman, J.P., 1989, "Experimental Methods for Engineers", Ed. McGraw-Hill, Singapore, Singapore.

Kays, W.M. and Crawford, M.E., 1980, "Convective Heat and Mass Transfer", 2º ed., Ed. McGraw-Hill.

Kern, D. Q., 1965, "Process Heat Transfer", Ed. McGraw-Hill, Singapore, Singapore.

Rowley, G.J. and Patankar, S.V., 1984, "Analysis of Laminar Flow and Heat Transfer in Tubes with Internal Circunferencial Fins", Int. J. of Heat Mass Transfer, Vol. 27, No. 4, pp. 583-560.

Versteeg, H. K. and Malalasekera, W., 1995, "An Introduction to Computational Fluid Dynamics", Ed. Prentice Hall.

Weeb, R.L., Eckert, E.R.G. and Goldstein, R.J., 1971, "Heat Transfer and Friction in Tubes with Repeated-Rib Roughness", Int. J. of Heat Mass Transfer, Vol. 14, pp. 601-617.

Williams, F. A. , 1985, "Combustion Theory", 2nd ed., Ed. Adison Wesley, USA.

Yuan, Z., Tao, W. and Wang, Q., 1998, "Numerical Prediction for Laminar Forced Convection Heat Transfer in Parallel plate channels with Streamwise-periodic Rod disturbances", Int. J. for Num. Methods in Fluids, Vol. 28, No 9, pp. 1371-1387.